



Swansea University  
Prifysgol Abertawe



## Cronfa - Swansea University Open Access Repository

---

This is an author produced version of a paper published in:

*Renewable Energy*

Cronfa URL for this paper:

<http://cronfa.swan.ac.uk/Record/cronfa34753>

---

### Paper:

Elasha, F., Mba, D., Togneri, M., Master, I. & Teixeira, J. (2017). A hybrid prognostic methodology for tidal turbine gearboxes. *Renewable Energy*

<http://dx.doi.org/10.1016/j.renene.2017.07.093>

---

This item is brought to you by Swansea University. Any person downloading material is agreeing to abide by the terms of the repository licence. Copies of full text items may be used or reproduced in any format or medium, without prior permission for personal research or study, educational or non-commercial purposes only. The copyright for any work remains with the original author unless otherwise specified. The full-text must not be sold in any format or medium without the formal permission of the copyright holder.

Permission for multiple reproductions should be obtained from the original author.

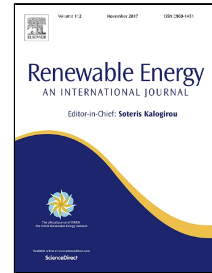
Authors are personally responsible for adhering to copyright and publisher restrictions when uploading content to the repository.

<http://www.swansea.ac.uk/iss/researchsupport/cronfa-support/>

# Accepted Manuscript

A hybrid prognostic methodology for tidal turbine gearboxes

Faris Elasha, David Mba, Michael Togneri, Ian Master, Joao Amaral Teixeira



PII: S0960-1481(17)30720-6  
DOI: 10.1016/j.renene.2017.07.093  
Reference: RENE 9068  
To appear in: *Renewable Energy*  
Received Date: 28 December 2015  
Revised Date: 14 December 2016  
Accepted Date: 23 July 2017

Please cite this article as: Faris Elasha, David Mba, Michael Togneri, Ian Master, Joao Amaral Teixeira, A hybrid prognostic methodology for tidal turbine gearboxes, *Renewable Energy* (2017), doi: 10.1016/j.renene.2017.07.093

This is a PDF file of an unedited manuscript that has been accepted for publication. As a service to our customers we are providing this early version of the manuscript. The manuscript will undergo copyediting, typesetting, and review of the resulting proof before it is published in its final form. Please note that during the production process errors may be discovered which could affect the content, and all legal disclaimers that apply to the journal pertain.

## A hybrid prognostic methodology for tidal turbine gearboxes

Faris Elasha<sup>1\*</sup>, David Mba<sup>2</sup>, Michael Togneri<sup>3</sup>, Ian Master<sup>3</sup>, Joao Amaral Teixeira<sup>4</sup>

<sup>1</sup>Faculty of Engineering, Environment and Computing , Coventry university, UK

<sup>2</sup>London South Bank University, London, UK

<sup>3</sup>Swansea University, Swansea, UK

<sup>4</sup>Cranfield University, Bedfordshire, UK

### ABSTRACT

Tidal energy is one of promising solutions for reducing greenhouse gas emissions and it is estimated that 100 TWh of electricity could be produced every year from suitable sites around the world. Although premature gearbox failures have plagued the wind turbine industry, and considerable research efforts continue to address this challenge, tidal turbine gearboxes are expected to experience higher mechanical failure rates given they will experience higher torque and thrust forces. In order to minimize the maintenance cost and prevent unexpected failures there exists a fundamental need for prognostic tools that can reliably estimate the current health and predict the future condition of the gearbox.

This paper presents a life assessment methodology for tidal turbine gearboxes which was developed with synthetic data generated using a blade element momentum theory (BEMT) model. The latter has been used extensively for performance and load modelling of tidal turbines. The prognostic model developed was validated using experimental data.

### Keywords

Tidal Turbines, Prognosis, Gearbox, Life Prediction, Diagnosis, Health management

---

\*Corresponding author. Tel: +44 (0) 2477659139.

E-mail address: [faris.elasha@coventry.ac.uk](mailto:faris.elasha@coventry.ac.uk) .

27

## 28 **1 Introduction**

29 Power generated from Renewable energy resources in the UK in 2015 increased by 29%  
30 compared to 2014, and accounted for 25 per cent of total UK electricity generation. Wave  
31 and tidal stream energy has the potential to meet up to 20% of the UK's current electricity  
32 demand, representing a 30-to-50 gigawatt (GW) installed capacity. Between 200 and 300  
33 megawatts (MWs) of generation capacity may be able to be deployed by 2020, and at the  
34 higher end of the range, up to 27GWs by 2050[1]. [2]. [3].

35

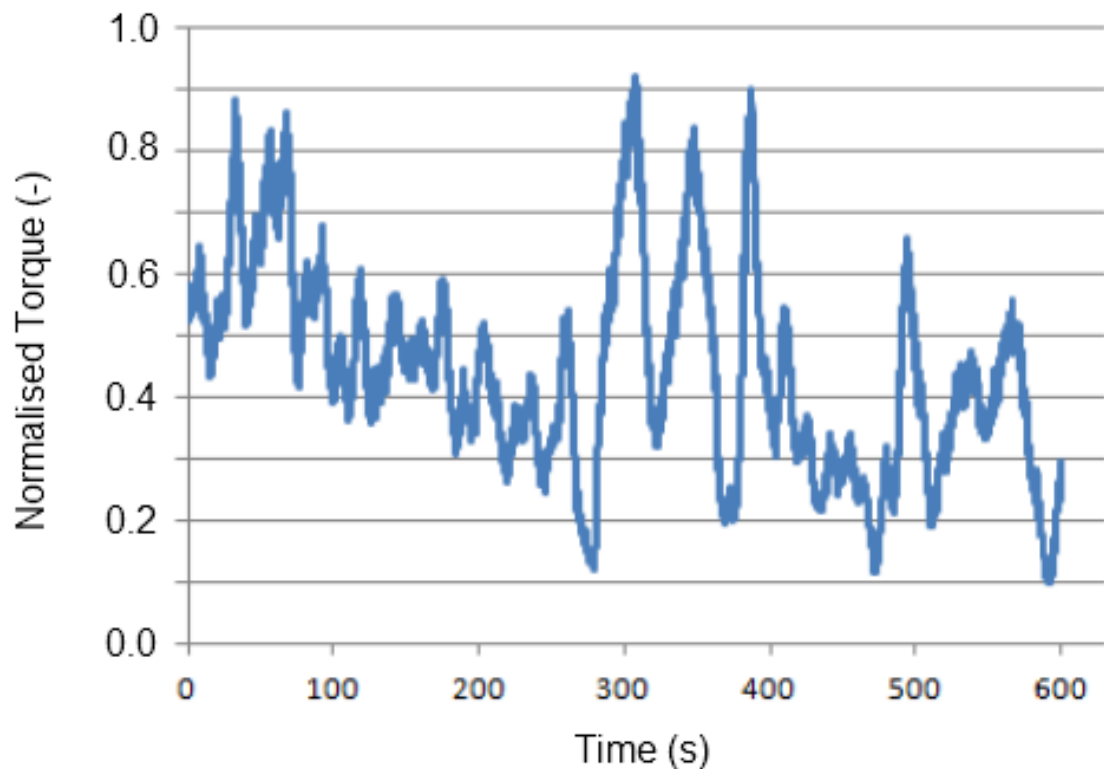
36 Operation and maintenance (O&M) decisions for tidal turbines contributes significantly to  
37 the cost of tidal energy production [4]. These decisions generally depend on many factors  
38 such as machine health, repair costs, weather conditions, etc. Premature failures in  
39 gearboxes result in a significant cost increase due to unplanned maintenance and long  
40 downtime. Such gearbox failures have plagued the wind turbine industry for decades  
41 despite reasonable adherence to design practices [5]. The tidal turbine gearbox will  
42 experience higher torque, thrust and transient events [6].

43

44 Recent wind industry experience has triggered the use of essentially three main  
45 approaches for dealing with gearbox reliability; root cause analysis, improving system  
46 design and condition monitoring [7, 8]. The Condition Monitoring (CM) systems of wind  
47 turbine gearboxes are commonly applied to detect damage in advance of the failure of  
48 the equipment. Efficient condition monitoring must be sensitive enough to detect potential  
49 failure events in order to provide adequate time for an operator to plan maintenance  
50 inspections and repairs [9-11]. Oil and vibration analysis have been used extensively for  
51 condition monitoring of wind turbine gearboxes [12-14]. These provide identification of  
52 changes in predetermined condition indicators (CI), and ideally should be capable of  
53 quantifying damage severity in order to estimate remaining useful life (RUL) using failure  
54 prediction models. Oil debris monitoring is more beneficial for fault identification as the

55 majority of faults in wind turbine gearboxes are due to bearing spall and gear pitting [13].  
56 These types of faults release metallic wear debris particles and the size and number of  
57 these particles increases with time until failure is reached. Recently a combination of oil  
58 and vibration analysis has been applied in order to efficiently predict the remaining life of  
59 bearings. This technique utilizes modern computational algorithms such as neural  
60 networks [15, 16], fuzzy logics [17] and a Bayesian network [18] to predict the failure.  
61 However, varying loads and speed fluctuations provide a challenge to the application of  
62 many of these algorithms [19, 20]. The availability of tidal turbines significantly affects  
63 their economic viability and a key aspect of tidal turbine availability is the need for efficient  
64 planning of maintenance resources. Condition Monitoring Systems (CMS) offer a solution  
65 to maintenance management and increased reliability [5, 21-23] as demonstrated in the  
66 wind turbine industry. Such systems continuously monitor turbine components and  
67 provide an optimum maintenance schedule.

68  
69 Failures in gearboxes are essentially related to the uncertainty associated with loading  
70 condition during the design phase. In addition transient loading events contribute  
71 detrimentally to fatigue life. These transient load events are caused by large variations  
72 in load condition, grid loss or resonant vibration. The former is of particular concern as  
73 the operational load variation on tidal blades has been seen to change by 100% within a  
74 few seconds, as depicted in Figure 1. In this instance the normalised torque increased  
75 from just over 0.1 to 0.9 within 10 seconds. These large variations in load have a  
76 determinant effect on drivetrain mechanical integrity, and as such the continuous  
77 monitoring of the tidal loading condition can provide an effective tool for health  
78 assessment [24].



79

80 Figure 1 Example of load variation on tidal blades based on flow prediction for Ramsy  
81 Sound site in the UK [25]

82

83 Generally, prognostic approaches can be categorized into three forms: data-driven,  
84 physics-based and fusion prognostics (hybrid) approaches. The majority of current  
85 research into gearbox prognosis uses the data-driven methodology which is based on  
86 vibration and oil analysis [9, 13, 26] technologies. Typically, the data is collected during  
87 operation and then statistically treated to estimate the residual life (RUL). However, for  
88 most of the developed prediction models the time between the residual life (RUL)  
89 prediction and actual failure is relatively short [27] which ultimately leads to higher  
90 maintenance costs. Physics-based models have been applied for prediction of life based  
91 on crack propagation theory; such models require significant information and are difficult  
92 to develop so they have not become established in industry [28]. Hybrid approaches

93 combine both data-driven and physics-based information to take the advantage of the  
94 strengths of each approach while overcoming their limitations [29].

95 This paper introduces a hybrid prognostic approach for predicting the remaining life  
96 centred on a methodology that combines data-driven and physics-based models. The aim  
97 of this paper is to propose this new methodology as a practical tool for gearbox prognosis.  
98 In order to predict the life accurately realistic data is required, therefore data based on  
99 a hydrodynamic model has been generated for demonstrating and validating the  
100 presented prognostic model; details of the hydrodynamic model is presented in section  
101 3.”.

102 This research presents a novel approach for gear prognosis which can be used for both  
103 wind and tidal turbines. The main contributions of this work includes residual gear life  
104 estimation for tidal gearboxes based on realistic load and speed conditions, which was  
105 generated for one of UK sites earmarked for tidal power. In addition, the paper introduces  
106 a new method to generate realistic flow data based on a combination of ADCP, SEM, and  
107 BEMT.

## 108 **2 Prognostic Concept**

109 Gearbox life is limited by the ability of the gear teeth to transmit power for the required  
110 number of cycles without failure. The most common gear failure modes are pitting,  
111 spalling and bending fatigue. Therefore, significant efforts have been made to minimize  
112 these failures at the design phase by considering different design characteristics.  
113 International standards for gear design [30, 31] consider the life of gears for both bending  
114 and contact fatigue. The latter leads to the formation of pits which occur if the limits of  
115 the surface durability of the meshing flanks are exceeded, resulting in particles breaking  
116 out of the flanks leading to pit formation. The extent to which such pits can be tolerated  
117 (in size and number) varies within wide limits, depending mainly on the field of application.  
118 In some fields, extensive pitting can be accepted; in other fields, any appreciable pitting  
119 is to be avoided. In bending fatigue, if the load exceeds the fatigue limit, cracks are

120 formed. The first of these often appears in the fillets where the compressive stress is  
121 generated; i.e. in the “compression fillets” which are those of the non-working flanks.  
122 Tooth breakage usually ends the service life of a transmission system. In this study, the  
123 gear failure initiation is considered as the point of end of life.

124  
125 The gear design process considers numerous influences that can be generalized into  
126 material factors, geometric factors, lubrication and general influence factors. These  
127 factors were introduced to take account of the influence of many characteristics of gears  
128 such as the elasticity of the material, the helix angle of the teeth and the number of cycles  
129 in the design life. These factors were categorized into three: general influence factors (K),  
130 pitting resistance factors (Z) and bending resistance factors (Y). The general influence  
131 factors are used in both pitting and tooth bending resistance calculations and includes the  
132 application factor  $K_A$ , which accounts for the effect of variable load, the dynamic factor  $K_v$ ,  
133 which makes allowance for the effects of gear tooth quality level and modifications relating  
134 to speed and load. Moreover, other load factors ( $K_{H\beta}$  and  $K_{H\alpha}$ ) are applied to take account  
135 of the influence of load distribution in both normal and transverse directions [30]. The  
136 pitting resistance factors include geometry factors which account for the influence of  
137 geometry characteristics to contact fatigue such as zone factor  $Z_H$ , helix angle factor  $Z_\beta$   
138 etc. In addition, pitting fatigue resistance factors account for the effect of material and oil  
139 film. An estimation methodology of pitting resistance factors is detailed in the relevant ISO  
140 standard (ISO 6336.2) [32]. The numerous bending fatigue resistance factors determine  
141 the effect of geometry and surface condition on gear root bending fatigue [33]. These  
142 influencing factors on gears life are considered in the prognostic methodology presented  
143 in this paper.

144  
145 The prognostic model presented aims to evaluate the remaining life of tidal turbine  
146 gearboxes. This model is focused on predicting the residual time before failure initiation.  
147 Failure initiation is characterised by the presence of the first pit on gear flank. The size of



148 this pit varies depending on gear modules, the gears module is the unit of size that  
149 indicates how big or small a gear is. It is the ratio of the reference diameter of the gear  
150 divided by the number of teeth, for gears with 2-5 module, the pit size that characterises  
151 a fault initiation is 0.4 mm in diameter [33]. For gears with modules above 5 the pit size is  
152 for fault initiation is 0.8 mm in diameter [34].

153

154 A schematic representation of the proposed prognostic model is shown in figure 2. The  
155 model consists of four stages; the first stage consists of processing measured data (rotor  
156 speed and torque) that is employed to estimate the drive train load spectra. The second  
157 stage includes gearbox design model which estimate gear geometry and fatigue  
158 resistance factors. The third stage brings together the load spectra, gear geometry and  
159 fatigue resistance factors into a life prediction model. At this stage a series of calculations  
160 are performed to estimate the gear damage index for pitting and bending failures, the  
161 damage index represents the fraction of life consumed by exposure to the cycles at the  
162 different stress levels. In general, when the damage fraction reaches 1, failure occurs. The  
163 last stage of the model involves predicting the remaining life is predicted based on the  
164 accumulated damage index and average damage index per tidal cycle, the later  
165 continuously updated through out turbine operation.

166

167

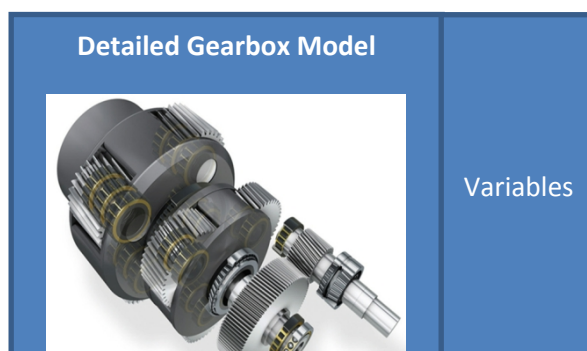
168

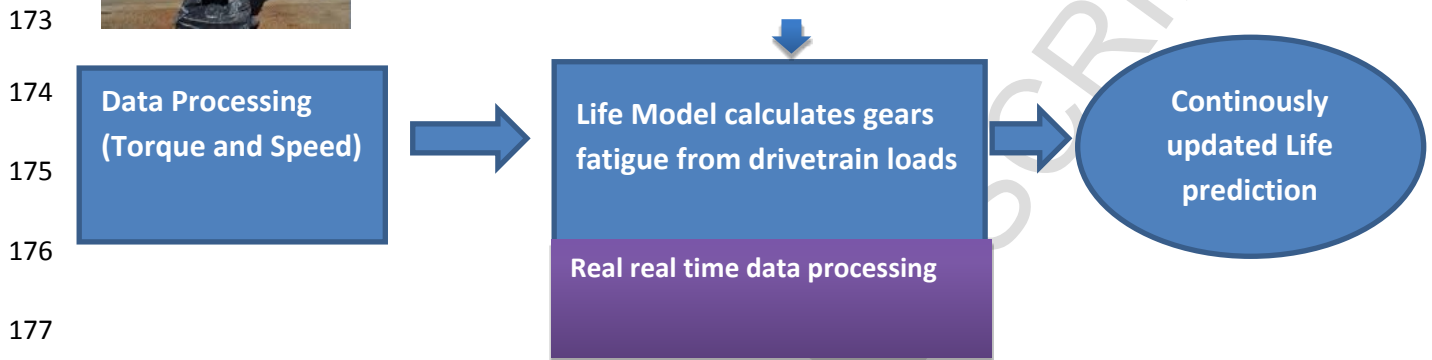
169

170

171

172





178 Figure 2 Gearbox prognostic model

179

180 To achieve life prediction model of tidal turbines understanding of gearbox design is  
 181 essential. The main function of the tidal turbine gearboxes is to transmit the power from  
 182 the low speed high torque rotor to the generator operating at high speed and low torque.  
 183 Typically epicyclic gear modules are employed due to their high transmission ratio, high  
 184 torque to weight ratio and high efficiency [35]. Tidal turbine gearboxes configurations are  
 185 similar to those employed in wind turbines as they share similar design features such as  
 186 the combined use of epicyclic and parallel gear configurations, see figure 3. The gearbox  
 187 configuration employed for this investigation consist of two planetary stages and one  
 188 parallel stage, see figure 3. The details of the gearbox design can be seen in table 1.  
 189 This gearbox type has been extensively studied to investigate premature wind turbine  
 190 gearbox failures [5, 8, 36-39], as such its application to the developed prognostic model  
 191 provided a source of validation.

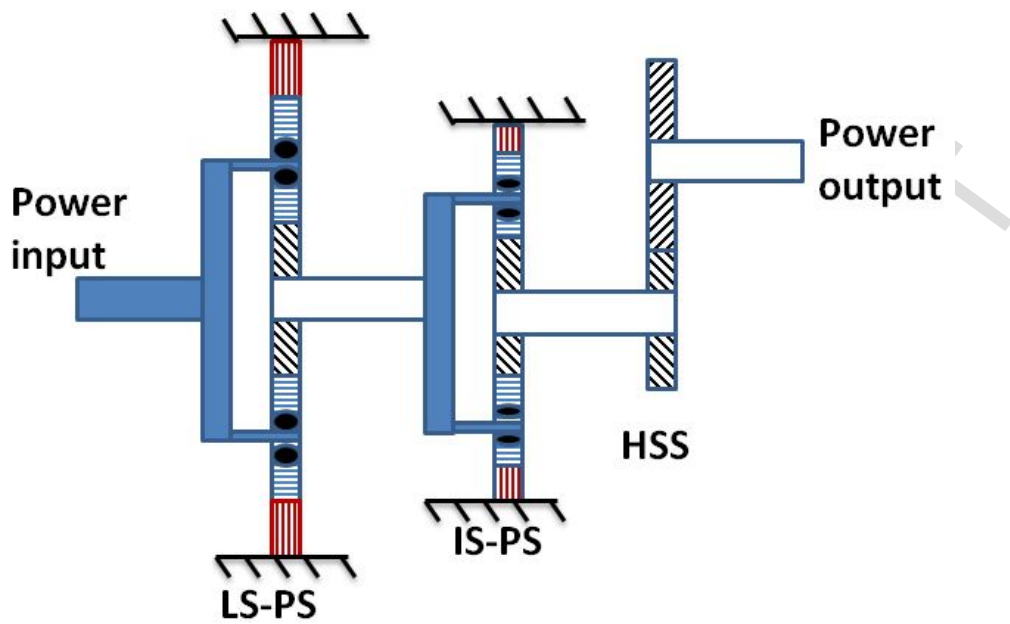


Figure 3 Gearbox configuration (LS-PS: Low Speed Planetary stage, IS-PS Intermediate Stage Planetary Stage, HSS: High Speed Stage) <sup>34</sup>

Table 1: Gearbox design features

Gear	Sun	Planet ( × 4)	Internal Gear
	First Stage		
Number of teeth	27	47	121

Module (mm)	8		
Helix angle (°)	0		
Facewidth (mm)	90		
Centre distance (mm)	296		
Second Stage			
Gear	Sun	Planet ( × 4)	Internal Gear
No teeth	25	23	75
Module (mm)	9		
Helix angle (°)	0		
Facewidth (mm)	98.5		
Centre distance (mm)	230		
Third stage			
Gear	Pinion		Wheel
No of teeth	18		69
Module (mm)	4		
Helix angle (°)	0		
Facewidth (mm)	54.945		
Centre distance (mm)	172		

## 202 2.1 Cycle counting

203 In the majority of applications gearboxes typically operate at rated torque throughout their  
 204 life and as such the predicted gear fatigue strength is modified by 'life factors' obtained  
 205 from the material characteristics. However for gearboxes subject to loads of differing  
 206 amplitude stress cycles counting is required. Many traditional techniques have been  
 207 suggested for stress cycles counting such as rainflow and rang-pair methods. However  
 208 for tidal gearboxes the number of stress cycles does not only depend on the variable  
 209 loading condition but also on the gear rotational speed, therefore the use of traditional  
 210 cycle counting methods are inappropriate. To overcome this limitation the authors used  
 211 the number of cycles at a particular stress level, estimated based on time spent at each  
 212 load and speed, see equation (1).

$$N_t = \frac{\omega_t}{60} \times \frac{1}{F_{\text{sample}}} \quad (1)$$

213 Where  $N_t$  is the number of cycles for one tooth of each gear,  $\omega_t$  (rpm) is the rotating speed  
214 of the gear during the corresponding load,  $F_{\text{sample}}$  is the fraction of time corresponding to  
215 the load under consideration.

216 Equation (1) shows the number of cycles  $N_t$  is calculated for each data sample, so the  
217 number cycle is calculated for each load point, which generate a very dense load  
218 spectrum (load-cycle spectrum). Therefore data reduction is important to avoid  
219 computationally expensive data processing. Data reduction was achieved by accumulation  
220 load cycles into a load spectrum with a larger bin size. The first step in constructing this  
221 spectrum is to divide the entire load range of values into a series of intervals and then  
222 count how many cycles at the same load fall into each interval.

223 Ideally the prognostic model should use data from operational measurements of torque  
224 and speed. However, for the purposes of this investigation, data from the numerical  
225 simulation described in section 3 was employed. With the torque data the corresponding  
226 load on gears were estimated using the ISO 6336 methodology [30, 31].

## 227 **2.2 Life Estimation**

228 It is well-known that contact and bending stress levels have a substantial effect on gear  
229 fatigue life. Fatigue failure takes place when these stresses exceed the permissible  
230 stresses. Estimation of these stresses involves consideration of fatigue resistance factors  
231 which account for the various influences on the life of the gears [32, 33]. The calculated  
232 service life is based on the notion that every load cycle contributes to the damage of the  
233 gears. The amount of damage depends on the stress level, with levels below a defined  
234 value considered as non-contributory.

235 Fatigue resistance factors are required for life estimation; these factors are calculated  
236 using the ISO standard based on gear geometric and material specifications. A numerical  
237 tool was used to extract these features based on Method C of ISO 6336. The factors are  
238 summarized in Table 2, the details and physical meaning of these factors can be found  
239 in [32, 33].

240

Table 2: Fatigue resistance factors calculated based on ISO guidelines

Parameter	Sun gear	Planet gears
Dynamic load $K_V$	1.001	
Transverse load factor (contact stress) $K_{H\beta}$	1.063	
Face load factor (root stress) $K_{F\beta}$	1.049	
Face load factor (contact stress) $K_{H\alpha} / K_{F\alpha}$	1	
Zone factor $Z_H$	2.495	
Single pair tooth contact factors $Z_{B/D}$	1.03	1
Elasticity factor $Z_E$	189.812	
Contact ratio factor $Z_\epsilon$	0.878	
Helix angle factor (contact) $Z_\beta$	1	
Life factor (contact) $Z_{NT}$	0.95	0.972
Lubricant factor (contact) $Z_L$	1.047	
Velocity factor $Z_V$	0.942	
Roughness factor $Z_R$	0.99	
Work hardening factor $Z_W$	1	
Size factor $Z_X$	1	
Tooth form factor $Y_F$	1.39	1.290
Stress correction factor $Y_S$	1.92	2.045
Stress correction factor $Y_{ST}$	2	
Helix angle factor (tooth root) $Y_\beta$	1	
Rim thickness factor $Y_B$	1	1
Deep tooth factor $Y_{DT}$	1	
Life factor (tooth root) $Y_{NT}$	0.91	0.928
Test relative notch sensitivity factor $Y_{\delta_{relT}}$	0.99	0.996
Relative surface factor $Y_{RrelT}$	1.04	1.047
Size factor (tooth root) $Y_X$	0.97	0.97
Mean stress influences factor $Y_M$	1	1
Safety factors in pitting	1.25	1.313
Safety factors in tooth bending	2.56	2.652

241

242 In order to estimate the gear life, bending and pitting stress spectra are required and this  
 243 is calculated based on the equation (2) [33].

$$\sigma_{fi} = 2000 \frac{T_i}{d_{ref} m_n b} Y_S Y_F Y_\beta K_{vi} K_{Bi} K_{\alpha_i} \quad (2)$$

244 Where  $T_i$  is the torque experienced by gear,  $\sigma_{fi}$  is nominal tooth root stress which is the  
 245 maximum local principal stress produced at the tooth root when an error-free gear pair is  
 246 loaded by the static nominal torque and without any pre-stress such as shrink fitting [33].

247 The contact stress spectrum is estimated by [32]:

$$\sigma_{Hi} = Z_H Z_E Z_{\epsilon} Z_{BD} \sqrt{2000 \frac{T_i}{d_{ref}^2 b} \frac{u+1}{u} K_{vi} K_{H\beta} K_{H\alpha}} \quad (3)$$

248 Where  $\sigma_{Hi}$  is the contact stress at pitch point which is the stress due to the static nominal  
 249 torque of error-free gears.

250 To account for variation of load distribution for the planetary gears the nominal stress  
 251 spectrum for bending and contact are corrected [30, 32, 33], see equations (4) and (5).

$$\sigma_H = Z_B \sigma_{Hi} \sqrt{K_A K_V K_{H\beta} K_{H\alpha}} \quad (4)$$

$$\sigma_F = \sigma_{Fi} K_A K_V K_{F\beta} K_{F\alpha} \quad (5)$$

252 All factors used in the above equations are defined in Table 2. These stress spectra  
 253 are used to estimate the life factors for pitting  $Z_{nt}$  and bending  $Y_{nt}$ .

$$Z_{nt} = \frac{\sigma_H}{\sigma_{HP}} \quad (6)$$

$$Y_{nt} = \frac{\sigma_{fi}}{\sigma_{fP}} \quad (7)$$

254 In turn, the life factor is used to estimate the corresponding number of cycles to failure for  
 255 each load bin using the graphical information in ISO 6336-2:2006, figure 6, and ISO 6336-  
 256 3:2006, Figure 9. Then, the damage index due to fatigue is calculated for each cycle using  
 257 the Miner's rule [34].

$$D = \sum_{i=0}^n \frac{N_t}{N_i} \quad (8)$$

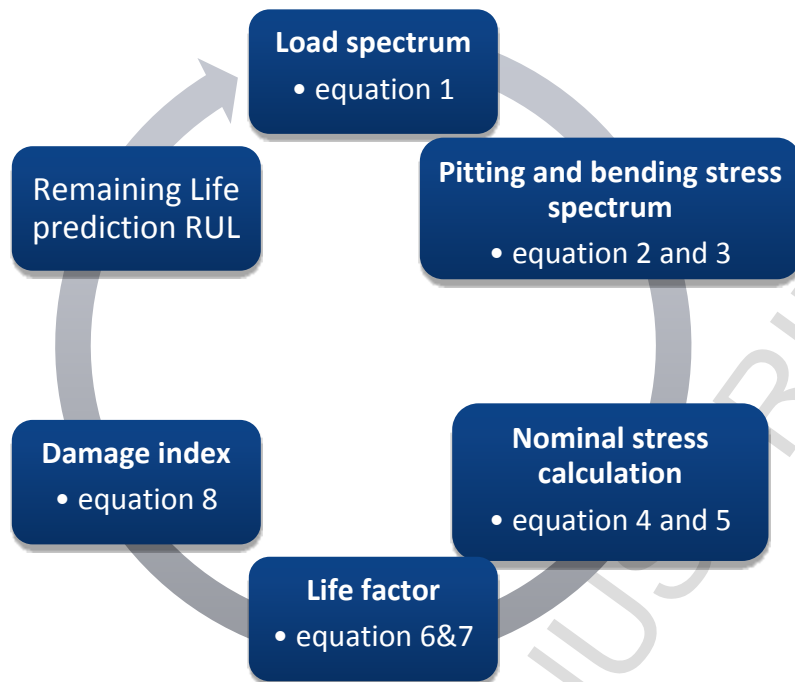
258 In which  $N_t$  is the number of cycles for one gear tooth and  $N_i$  is the total number of cycles  
 259 in order to cause damage under corresponding loading conditions. This is estimated  
 260 based on material fatigue characteristics described by the Wohler curve, as derived from  
 261 material testing under cyclic loading. The test results are presented as a plot of stress (S)  
 262 against the number of cycles to failure (N), known as an S-N curve; the international  
 263 standard provides this data for gears material for both contact and bending stresses (ISO  
 264 6336-2:2006, and ISO 6336-3:2006) [32, 33].

265  
 266 Remaining life prediction of gears are not only dependent on the load history experienced  
 267 by the turbine , but also the expected future load. As the tidal cycle can be accurately  
 268 predicted for specified locations using hydrodynamic ocean modelling system, see [40] ,  
 269 therefore the average damage index per the tidal cycles  $D_a$  can be estimated using a load  
 270 history. For purpose of this study the average damage index is calculated based on one  
 271 tidal cycle due to lack of longer hydrodynamic data, however using longer hydrodynamic  
 272 data could lead to more accurate average damage index per tidal cycle. The remaining  
 273 life (L) is predicted by:

$$L = \frac{1 - D}{D_a} \quad (9)$$

274  
 275  
 276 The process of predicting the life described above is a continuous process and suitable  
 277 for online gearbox prognostics as summarised in Figure 4.





278

279

Figure 4 The proposed prognostic process

280

### 281 3 Hydrodynamic modelling

#### 282 3.1 Blade element momentum theory (BEMT)

283

284 The synthetic torque records used in this paper were generated using a blade element  
 285 momentum theory (BEMT) model of a tidal turbine. BEMT is a widely-employed technique  
 286 [41-43] for modelling conventional horizontal-axis turbines, in both wind and tidal  
 287 application. There is an extensive and well-rooted literature on the method [44] so a brief  
 288 overview is presented here.

289 In essence, BEMT parameterises two different models of a turbine with parameters called  
 290 'induction factors', and then determines the value of the induction factors that brings these  
 291 models into agreement. In the first place, the turbine was represented as a collection of  
 292 annular rings, each of which absorbs some linear momentum from the flow of the fluid

293 and imparts a degree of swirl into the wake. In the second place, the turbine was regarded  
294 as a collection of two-dimensional foils generating lift and drag forces that vary depending  
295 on the flow angle and velocity at the foil location. The annuli in the first representation and  
296 the blade elements in the second lie at the same radial locations, giving a one-to-one  
297 correspondence. The lift and drag coefficients are calculated from a lookup table that is  
298 chosen based on the specific foil used in the turbine design, and the forces themselves  
299 also depend on the chord length and angle of blade twist at each radial location.

300 The two induction factors (axial and tangential) indicate how much the momentum flux of  
301 the working fluid through each annular element is changed by the presence of the blades;  
302 they also affect the velocity of the fluid relative to each blade element and thus determine  
303 the hydrodynamic forces. Since the change of momentum flux and the hydrodynamic  
304 forces must be equivalent, the problem is reduced to finding the values of the induction  
305 factors that satisfy this requirement. There are a number of approaches to solving this  
306 problem; the method employed [43] treats it as a minimisation problem.

307 The BEMT is most commonly used to predict turbine performance in terms of power  
308 output. However, as the forces on each of the blade elements were calculated at each  
309 time step of the simulation the time-varying loads on the rotor can be calculated  
310 throughout the duration of the simulation by summing the tangential forces across all  
311 blades. This method has been employed to generate the torque records used in the  
312 current study. Although classical BEMT only allows steady uniform inflow, the model  
313 employed has been modified such that it can simulate a turbine subject to non-uniform,  
314 time-varying flows.

315

316

317

318

### 319 3.2 Synthetic Eddy Method (SEM)

320

321 Classical BEMT requires a steady, uniform inflow. In this new modified model, the ability  
322 to track the location of each two-dimensional foil has been added on each blade  
323 separately, allowing the simulation of unsteady and non-uniform flows. This capability  
324 allows out the work described in this paper to be carried.

325 This capability, of course, is of limited use if appropriate inflow data is not available.  
326 Ideally, measured field data should be used from a turbine deployment site; however,  
327 there is no device capable of taking simultaneous, high-frequency measurements of all  
328 three components of flow velocity across a volume of water large enough to contain a full-  
329 scale turbine. Instead, the synthetic eddy method (SEM) was employed to generate an  
330 artificial flow field that can be specified to arbitrary precision in both space and time.

331 The SEM was developed as a way of generating inflow data for Large Eddy Numerical  
332 simulations [45]. Again, an extensive description of SEM is beyond the scope of the  
333 current work, so a brief description only is provided here. Given a set of covariances for  
334 the fluctuation velocities of a turbulent flow field, along with a distribution of eddy length  
335 scales, SEM generates a time-varying field of eddies each of which induce velocities in a  
336 region of space near them. The input data requirements are easily met, as the most  
337 common method of gathering data on turbulence at planned deployment sites is with  
338 acoustic Doppler current profilers [46-48], and these measurement devices output  
339 precisely the type of statistical data that SEM requires as an input.

340

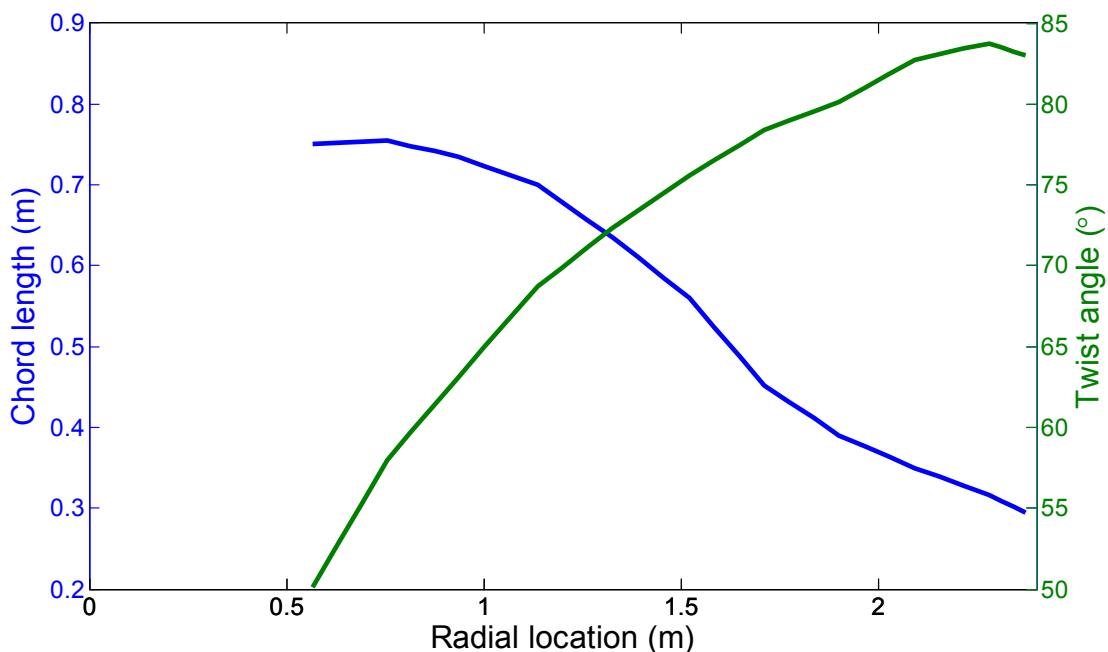
341 The synthetic eddies are characterised by a strength, which determines the magnitude of  
342 the induced velocities; a length scale, which determines the size of the region in which  
343 the eddies influence is present; and a shape function. With strengths derived from the  
344 input covariances and a suitably-normed shape function (see [45] for details), the second-  
345 order statistical moments of the artificial flow field will match those specified by the

346 covariances used to calculate the eddy strengths. Note that this matching is only exact  
 347 for a simulated flow-field of infinite duration.

348

#### 349 **4 Generation of the torque record**

350 The geometry of a model turbine that has been extensively tested was employed in this  
 351 study [49]. The model itself is too small to be effectively used in turbulent flows based on  
 352 field data, as it would be significantly smaller than the smallest measured eddy length  
 353 scales; therefore the authors elected to scale up the radius and chord length by a factor  
 354 of 10, giving an overall rotor diameter of 4.75m. The geometry characteristics of the  
 355 blades of this turbine are shown in Figure 5; a Wortmann FX 63-137 blade section is used  
 356 for the entire blade span.



357

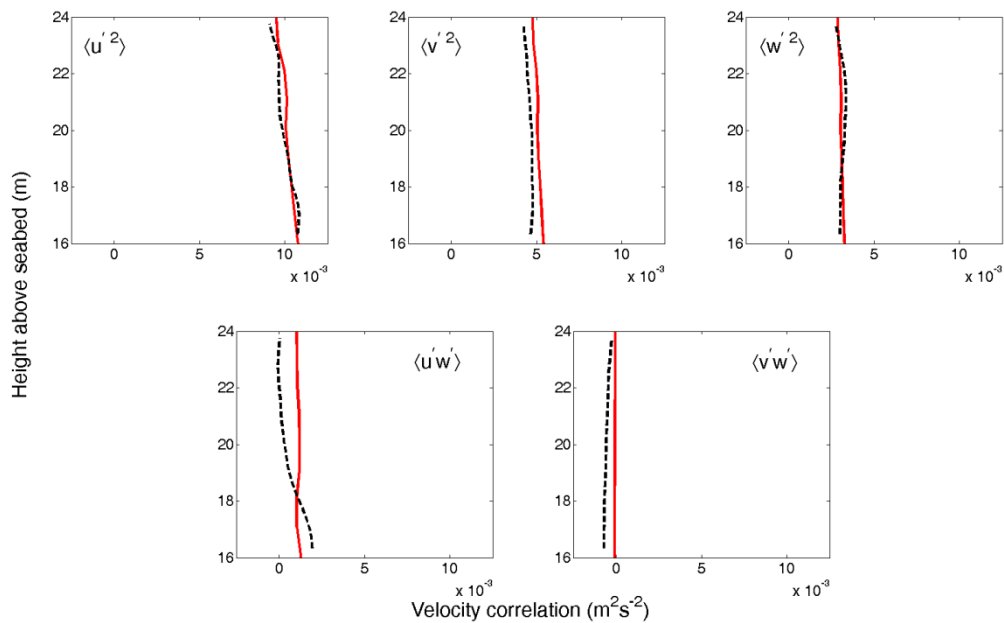
358 **Figure 5 Geometry characteristics of turbine blades used in the BEMT model.**

359

360 The Synthetic eddy method (SEM) was used to generate the inflow conditions based on  
361 measured field data. This field data used was taken from ADCP measurements in  
362 Ramsey Sound, a channel off the coast of Pembrokeshire, between the 13th and 27th of  
363 September, 2009; this encompasses a complete spring-neap cycle. Seven flood and ebb  
364 phases (i.e., fourteen phases in total) corresponding to regular intervals from the  
365 measurement period were selected as the test conditions for the work presented here.  
366 For each of these phases, the covariances needed to generate a synthetic turbulent field  
367 with SEM were calculated from an hour-long subset of ADCP data corresponding to the  
368 time of maximum current speed.

369

370 A full, three-dimensional velocity field of ten minutes duration was generated from each  
371 of the fourteen sets of turbulence statistics. Figure 6 shows an example of how the  
372 'template' statistics taken from ADCP measurements are replicated in the synthetic  
373 turbulence field, the top three panels show autocovariance for each of the three velocity  
374 fluctuation components ( $u'$ ,  $v'$  and  $w'$ ) and the bottom two panels show horizontal-vertical  
375 cross-covariance ( $u'w'$  and  $v'w'$ ), note that ADCPs cannot measure the horizontal-  
376 horizontal cross-covariance  $\langle u'v' \rangle$ ; this is set to zero in the SEM model. The data for this  
377 example were taken from the first ebb phase of the spring-neap cycle considered.  
378 Complete knowledge of the flow velocities at any point was provided by the synthetic flow  
379 field. Therefore the covariances were calculated directly, by taking the time-average of  
380 the velocity fluctuation products over the duration of the synthetic flow field. The results  
381 show that the measured velocity covariances are well replicated by the SEM. By running  
382 one BEMT simulation for each of the velocity fields generated in this way, torque records  
383 were obtained and then used as inputs for the gearbox prognostic model.



384

385 **Figure 6 Comparison of ADCP-measured turbulence statistics (solid red line) and**  
 386 **statistics of synthetic turbulence created using SEM (dashed black line) for a**  
 387 **representative tidal phase.**

388

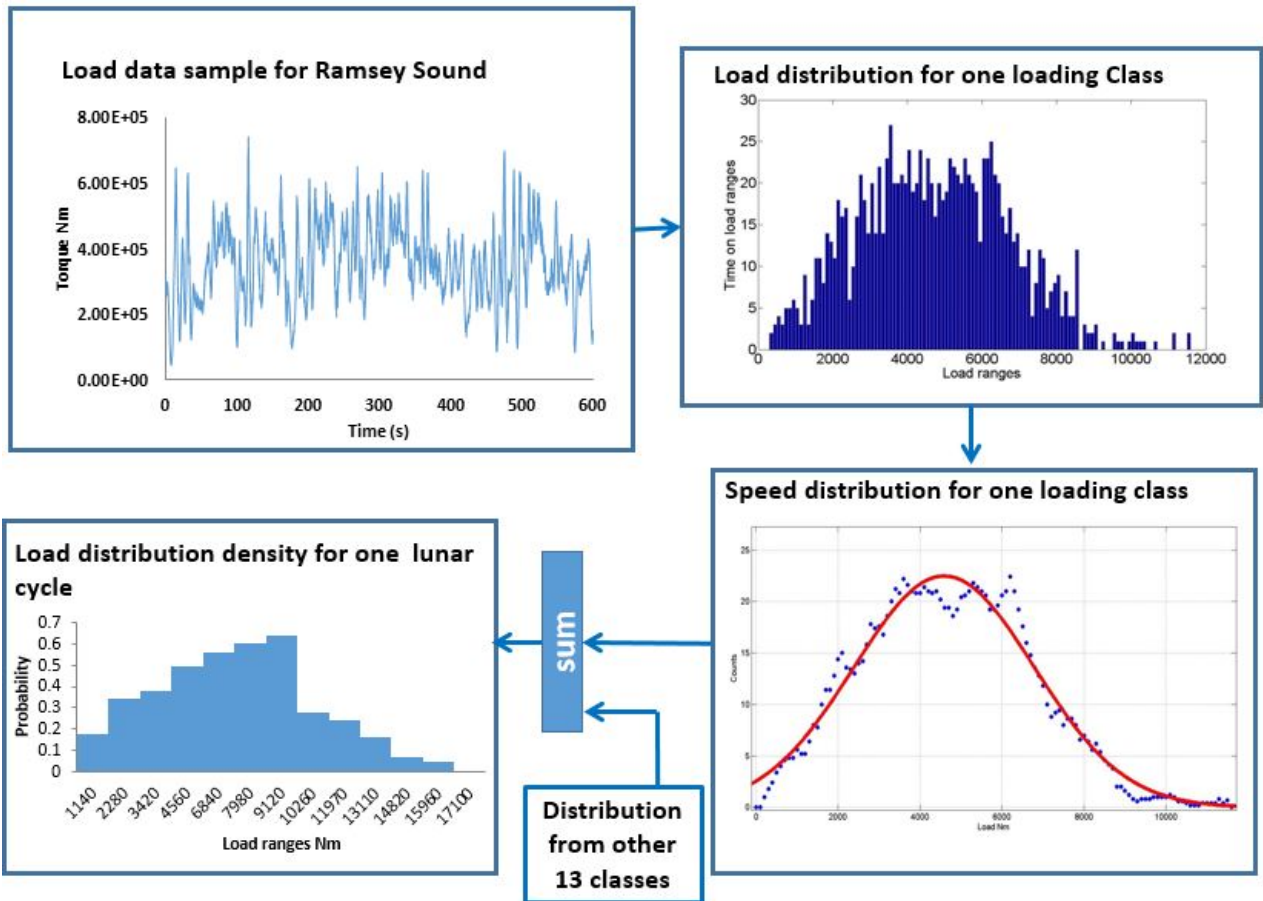
## 389 5 Data processing

390 The numerically simulated data was classified into ebb and flood groups based on flow  
 391 direction; flood corresponding to the tide flow into shore while ebb refers to the tide  
 392 draining away from shore. Each flow was assumed to represent 50% of the lifetime and  
 393 each flow contained 7 load classes, each class being represented by ten minutes speed  
 394 and torque data. The flow data used represents no-wave conditions.

395 The measured tide speed [24] was employed in the numerical simulation for generating  
 396 turbine speed and torque data for one tidal cycle (14 days). This provided the load  
 397 experienced by the transmission gearbox. A probability density function of the load was  
 398 estimated by considering the cycle during each of the seven load classes which was then  
 399 accumulated. This procedure was applied for both load and speed data as shown in

400 Figure 6 and Figure 7. The load and speed probability distribution was used as the basis  
 401 for predicting the load experienced by the gearbox throughout its life.

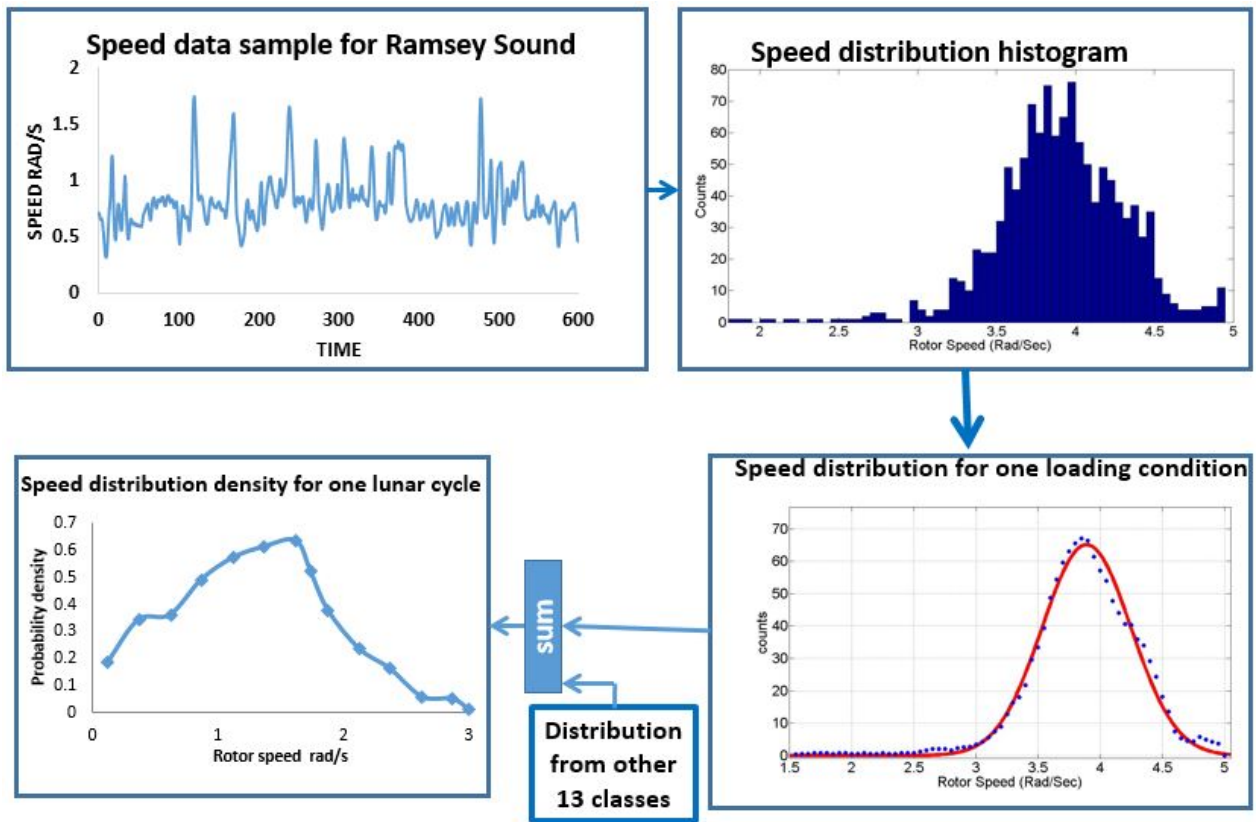
402



403

404

Figure 7 Load data processing



405

406

Figure 8 Speed data processing

## 407 6 Model output

408 The torque data from the numerical simulation was used to estimate the useful life based  
 409 on the procedure described above. The calculations began by estimating the load spectra  
 410 on the gears from the simulated torque and speed data. For the purposes of this  
 411 illustration it was assumed the gearbox was 100% efficient. The stress spectra for both  
 412 contact and bending were then determined from the load spectra, see Figure 9.

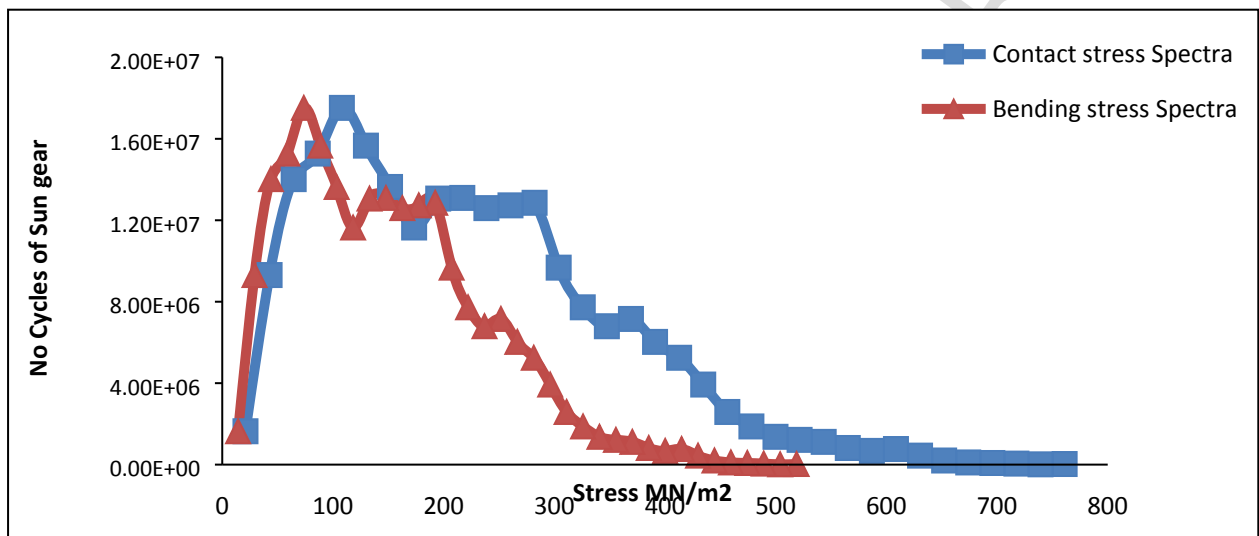
413

414 The stress spectra, geometric features, fatigue resistance factors and the equations  
 415 described previously were employed for estimating the damage index. For demonstration  
 416 purpose the result of first stage sun gear is summarised in figure 9 and table 3.



417 The analysis of the result shows that the sun gear of the first stage has a higher damage  
 418 index for contact load (0.0032 )compared to the bending load damage index (0.0026). In  
 419 addition the contact stress was higher than the bending stress (Figure 9) suggesting the  
 420 gears are expected to fail due to pitting as opposed to a tooth bending failure; the  
 421 expected life of first stage sun gear under these loading conditions is 157 lunar cycle  
 422 which corresponds to approximately 13 years.

423



424

425 **Figure 9 Sun gear stress spectrum over one tidal cycle**

426

427

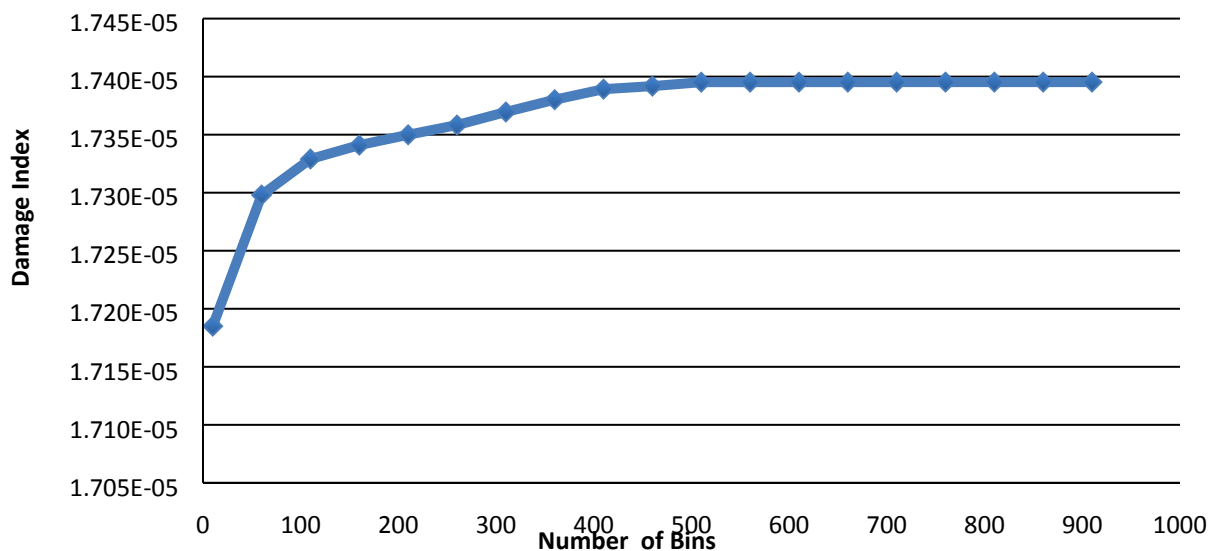
428

429 **Table 3 First stage sun gear life**

Sun Gear pitting life	157.8 lunar cycles
Sun Gear Bending life	194.82 lunar cycles
Sun Gear pitting Damage index for over one lunar cycle	0.0032
Sun Gear Bending Damage index consumption over one lunar cycle	0.0026

429

430 Load cycle data reduction has an impact on the accumulated damage index, therefore a  
431 sensitivity analysis on the effect of bin size when estimating the damage index was  
432 performed; the analysis was applied on the first stage sun gear and employed for one of  
433 load classes. The damage index was calculated using the different bin sizes of load  
434 spectrum. Following analysis it was noted that the use of a low number of bins results in  
435 overestimating of life, and at higher number of bins the damage index converges towards  
436 a constant damage index value, see Figure 10. However the difference between lower  
437 and higher values of bin size is not significant (less than 1.2%), see Figure 11. This implies  
438 that the choice of bin size has a minor effect on life prediction.  
439

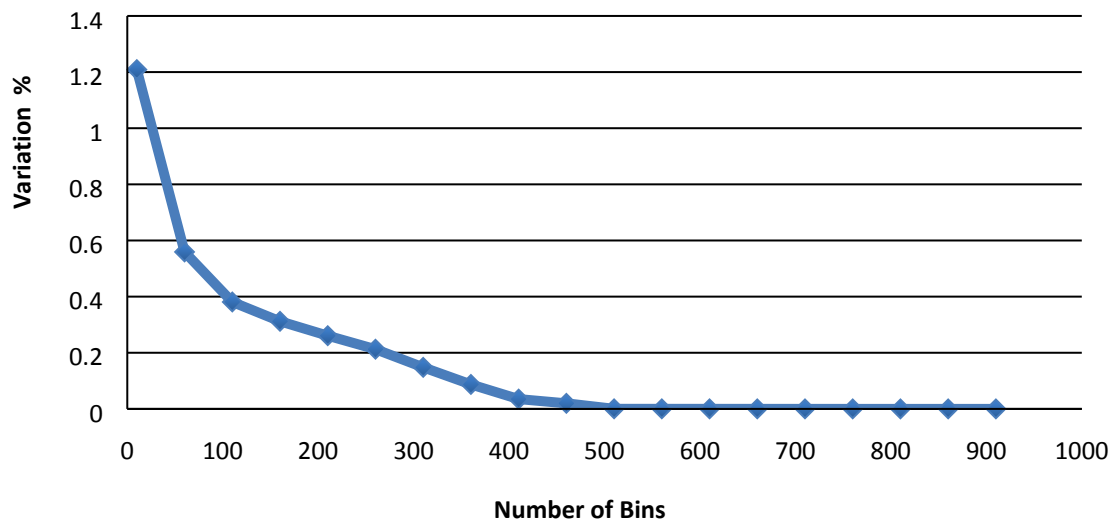


440

441

Figure 10 Damage index convergence

442



443

444

**Figure 11: Variation of result under different numbers of bins**

445

446 The analysis described thus far, as applied to the sun gear, was then employed to all  
 447 gears in the different stages within the gearbox. The results are summarised in table 4,  
 448 and shows that the 3<sup>rd</sup> parallel stage has the shortest life whilst the highest damage index  
 449 was noted on gears with the highest speed and smallest gear geometry. In addition results  
 450 showed that the ring gears have a longer life due to the larger gear size. The result shows  
 451 variations in the life and damage index of the gears which originate from geometrical  
 452 variability and differences in stress cycles due to the differing rotational speeds.

453

454

455

456

457

458

459

460

461

462

**Table 4: Result of life prediction for gearbox component**

<b>Components</b>	<b>Pitting life (No of lunar cycles)</b>	<b>Bending life (No of lunar cycles)</b>	<b>Pitting Damage index for over one lunar cycles</b>	<b>Bending Damage index for over one lunar cycles</b>
Planets gear(1st stage)	232.05	335.82	0.0023	0.0014
Sun gear (1st stage)	157.8	194.8	0.0033	0.00257
Ring Gear (1st stage)	347.16	487.05	0.0015	0.0010
Planets gear(2nd stage)	238.25	356.8	0.0021	0.0001
Sun gear (2nd stage)	162.01	207.0	0.00311	0.0024
Ring Gear (2 <sup>nd</sup> stage)	356.91	518.3	0.0014	0.0009
Pinion gear HSS	135.0	177.0	0.0038	0.0028
Wheel gear HSS	145.8	180.9	0.0035	0.0028

463

## 464 **7 Experimental demonstration**

465 It was thought prudent to perform some validation of the proposed prognostic model. The  
 466 validation was based on tests performed by Khan et al. [50] in which two pitting tests were  
 467 performed on two identical pairs of case-hardened low carbon steel gears. The gears  
 468 were tested under two loading conditions and the useful life was estimated based on ISO  
 469 6336-2 guidelines as described previously. The details of the gears used and the load  
 470 conditions are summarized in Table 5.

471

472

473

474

475

**Table 5: Gear parameter according to design calculation (ISO6336.2) [50]**

<b>Gear</b>	<b>Specification</b>
Helix angle	17.75 deg
Centre to distance	113.0 mm
No. of teeth	35.0
Reference diameter	110.2 mm
Load condition 1	6500 N
Load condition 2	4347 N
Speed	1000 RPM
Life estimated in load condition 1	$5.985 \times 10^5$ cycles
Life estimated in load condition 2	$9.67 \times 10^5$ cycles

476

477 The gear geometry and load conditions presented [48] were applied to the prognostic  
 478 model developed by the authors and results showed pitting when the number of cycles  
 479 reached  $5.4 \times 10^5$  cycles during the first load condition and  $1.08 \times 10^6$  cycles for the second  
 480 load condition. Applying the Miner's sum using equation (3), the damage level was  
 481 estimated at 0.92 for test 1 and 1.034 for test 2, (see **Table 6**). Visible pitting after gear  
 482 testing is shown in Figure 12 and Figure 13. Observations from Figure 12 and Figure 13  
 483 show the presence of small pits at a time when the corresponding value of the Miner's  
 484 sum (damage index) was approximately 1. This observation offered validation of the  
 485 proposed prognostic methodology albeit at fixed load conditions.

486

487

488

**Table 6: Model demonstration result**

	Test No. 1	Test No. 2
Actual Number of Cycles (from the test)	$5.9 \times 10^5$	$9.67 \times 10^5$
Predicted Number of Cycles	$5.4 \times 10^5$	$1.08 \times 10^6$
Predicted Damage Index	0.92	1.034



489

490

**Figure 12 Visible pitting after test 1 [50]**

491

492

**Figure 13 Visible damage after test 2 [50]**

493

494

495 **8 Discussion**

496 It has been shown that unsteady BEMT, in conjunction with SEM, can be used to predict  
497 some turbulence effects on TSTs, and to investigate how these effects can be  
498 ameliorated. The synthetic eddy method has been shown in figures 4 and 5 to yield a  
499 velocity field that, while non-physical, statistically reproduces measured turbulence. This  
500 means this research was able to simulate a Tidal Stream Turbine's TST response to  
501 turbulence of known statistical properties without the need for either detailed velocity  
502 measurements or expensive computation.

503 The synthetic eddy method, although it provides satisfactory turbulent flowfields in a  
504 statistical sense, is not the only way of predicting fluctuating velocities on a TST. There  
505 are well-validated spectral methods that are widely used in the wind turbine industry, and  
506 some recent work has indicated that the spectral properties of tidal currents are  
507 sufficiently similar that these atmospheric methods could be adapted for use in marine  
508 flows [51]. A fruitful avenue of research, then, would be to attempt analysis of the test  
509 cases presented in this paper in the case where artificial turbulence is generated with  
510 spectral methods adapted for tidal flow, rather than with SEM.

511

512 The prognostics model developed focuses only on fatigue damage due to the contact  
513 and bending stresses. However, it should be noted that the effect of data sampling  
514 frequency in this analysis can lead to life overestimation due to the low sampling rate of  
515 synthetic data employed, especially for the high speed stage where a higher sampling  
516 frequency is required. The ISO standard for cycle counting states that [52], "The sampling  
517 frequency shall be such that every analog loading cycle is represented by at least 20  
518 digital points at least 20 times that of the observed maximum frequency of the real or  
519 expected analog signal". The sampling frequency for the data employed was 20 Hz,  
520 which satisfied the requirement for analysis of the low speed gearbox stage. However for  
521 the high speed gear stages a sampling frequency 20 times the rotational frequency (24

522 Hz) is required, and therefore the life expectancy of the high speed stage should be  
523 calculated with a higher sampled torque data which was not available for this  
524 investigation. Even with the known life overestimation, the high speed stage (HSS) life  
525 was shorter than the other stages, and therefore damage is expected to initiate firstly in  
526 the gears of the high speed stage. This finding supports the observations of wind turbines  
527 failure, in which HSS failure were the most [53]. This is beneficial in not only giving an  
528 estimate for when maintenance ought to be scheduled, but also in identification of which  
529 components need to be redesigned or improved to lengthen the gearbox's fatigue life. It  
530 is worth considering that eleven years may be too pessimistic an estimate for the gear's  
531 lifespan, due to the fact that the probability distributions of load and speed that have been  
532 used are based on data from the fastest segments of flood and ebb phases across the  
533 spring-neap cycle, and thus they neglect both slack water and the less-intense portions  
534 of floods and ebbs. A probability distribution of loads that did incorporate these times with  
535 lower loading would almost certainly yield a longer fatigue life.

536

537 The gear life prediction results showed that the transmission system exposed to tidal  
538 currents will experience a shorter life compared to that exposed to wind load conditions.  
539 The gearbox considered in this study was designed to operate for 20 years (1.5-2 MW)  
540 however this analysis showed a 13 year life expectancy if this gearbox was employed in  
541 a tidal turbine, reiterating the influence on gear life for the very different loading conditions.  
542 The prognostic concept was validated using constant load experimental data, however  
543 further experimental work is recommended to assess the prognostic model under variable  
544 load conditions.

545

546



## 547 9 Conclusion

548 A prognostic model based on the loading condition has been developed to predict the  
549 residual life of a gearbox during turbine operation. The model employed synthetic  
550 turbulence data generated for The Ramsey Sound region [25]. The prediction model  
551 encompass an element of a physic based (fracture mechanics) and data driven  
552 approach. The result shows life variations between the gears. These variations come from  
553 geometrical variability and differences in stress cycles due to the differing rotational  
554 speeds.

555 Furthermore it was noted that the high speed pinion has the highest damage index. This  
556 is mainly due to its higher number of cycles and lower number of teeth compared to the  
557 other gears. In addition the progression of surface pitting damage is expected prior to  
558 any damage at the gear root.

559 This study emphasizes that the life prediction depends on probability of loading condition,  
560 therefore a statistical significant data set will enhance prediction. In addition continuous  
561 updates of load cycle during the turbine operation will contribute to life prediction  
562 accuracy. The model was validated using constant load pitting test data and an accurate  
563 prediction of life was proved. However further experimental investigation is recommended  
564 to verify the effect of variable load and speed.

565

566 **Acknowledgments:** The authors would like to thank the SuperGen UK Centre for Marine  
567 Energy Research (UKCMER) for funding this research (**EPSRC Grant EP/J010200/1**).

568

569 **References**

- 570 [1] *Digest of UK energy Statistics 2012*, (2012), 12/089, Department of Energy and Climate Change, UK.
- 571 [2] Department of Trade and Industry (2007), *Economic Viability of a Simple Tidal Stream Energy*  
572 *CAPTURE DEVICE*, TP/3/ERG/6/1/15527/REP, 2007, UK.
- 573 [3] Ben Elghali, S. E., Benbouzid, M. E. H. and Charpentier, J. F. (2007), "Marine Tidal Current Electric  
574 Power Generation Technology: State of the Art and Current Status", *Electric Machines & Drives*  
575 *Conference, 2007. IEMDC '07. IEEE International*, Vol. 2, pp. 1407.
- 576 [4] Houde, J. (2012), *Cost-benefit analysis of tidal energy generation in Nova Scotia: A scenario for tidal*  
577 *farm with 300 MW of installed capacity in the Minas passage in 2020* (Master thesis), Dalhousie  
578 University, Canada.
- 579 [5] Tavner, P. J., Xiang, J. and Spinato, F. (2007), "Reliability analysis for wind turbines", *Wind Energy*,  
580 vol. 10, no. 1, pp. 1-18.
- 581 [6] Winter, A. I. (2011), "Differences in fundamental design drivers for wind and tidal turbines", *OCEANS*,  
582 *2011 IEEE*, 6-9 June 2011, Santander, Spain, uk, pp. 1.
- 583 [7] Rao, B. (1996), *Handbook of condition Monitoring*, Elsevier, Oxford, UK, ISBN 185617 234 1.
- 584 [8] Spinato, F., Tavner, P. J., van Bussel, G. J. W. and Koutoulakos, E. (2009), "Reliability of wind turbine  
585 subassemblies", *Renewable Power Generation, IET*, vol. 3, no. 4, pp. 387-401.
- 586 [9] Dupuis, R. (2010), "Application of oil debris monitoring for wind turbine gearbox prognostics and  
587 health management", *Annual Conference of the prognostics and health management society*, 10-16  
588 October, Portland, pp. 10.
- 589 [10] Crabtree, C., James (2011), *Condition Monitoring Techniques for Wind Turbines* (Doctoral thesis  
590 thesis), Durham University, UK.
- 591 [11] Hameed, Z., Hong, Y. S., Cho, Y. M., Ahn, S. H. and Song, C. K. (2009), "Condition monitoring and  
592 fault detection of wind turbines and related algorithms: A review", *Renewable and Sustainable*  
593 *Energy Reviews*, vol. 13, no. 1, pp. 1-39.
- 594 [12] Wenxian Yang, Tavner, P. J., Crabtree, C. J. and Wilkinson, M. (2010), "Cost-Effective Condition  
595 Monitoring for Wind Turbines", *Industrial Electronics, IEEE Transactions on*, vol. 57, no. 1, pp. 263-  
596 271.
- 597 [13] Kitaljevich, D., Dupuis, R. and Lu, M. (2009), "Oil Debris Condition Monitoring for Wind Turbine  
598 Gearboxes", *Beijing Wind Power*, 21-23 October, Beijing, China, .

- 599 [14] Sait, A. and Sharaf-Eldeen, Y. (2011), "A Review of Gearbox Condition Monitoring Based on  
600 vibration Analysis Techniques Diagnostics and Prognostics", in Proulx, T. (ed.) *Rotating Machinery,*  
601 *Structural Health Monitoring, Shock and Vibration, Volume 5*, Springer New York, , pp. 307-324, ISBN  
602 978-1-4419-9427-1.
- 603 [15] Tse, P. W. and Atherton, D. P. (1999), "Prediction of machine deterioration using vibration based  
604 fault trends and recurrent neural networks", *Journal of Vibration and Acoustics, Transactions of the*  
605 *ASME*, vol. 121, no. 3, pp. 355-362.
- 606 [16] Venkatasubramanian, V., Vaidyanathan, R. and Yamamoto, Y. (1990), "Process fault detection and  
607 diagnosis using neural networks—I. steady-state processes", *Computers & Chemical Engineering*, vol.  
608 14, no. 7, pp. 699-712.
- 609 [17] Xiaoli Li, Shiu Kit Tso and Jun Wang (2000), "Real-time tool condition monitoring using wavelet  
610 transforms and fuzzy techniques", *Systems, Man, and Cybernetics, Part C: Applications and Reviews,*  
611 *IEEE Transactions on*, vol. 30, no. 3, pp. 352-357.
- 612 [18] Chen, B., Tavner, P. J., Feng, Y., Song, W. W. and Qiu, Y. (2012), "Bayesian network for wind turbine  
613 fault diagnosis.", *Proceedings of european wind energy association*, 16-19 April, Copenhagen,  
614 Denmark, European Wind Energy Association, .
- 615 [19] Elasha, F., Mba, D. and Ruiz-Carcel, C. (2016), "A comparative study of adaptive filters in detecting  
616 a naturally degraded bearing within a gearbox", *Case Studies in Mechanical Systems and Signal*  
617 *Processing*, vol. 3, pp. 1-8.
- 618 [20] Elasha, F., Greaves, M. and Mba, D. (2016), "Diagnostics of a Defective Bearing Within a Planetary  
619 Gearbox with Vibration and Acoustic Emission", in Chaari, F., Zimroz, R., Bartelmus, W., et al (eds.)  
620 Springer International Publishing, , pp. 399-412, ISBN 978-3-319-20462-8.
- 621 [21] Kacprzyński, G. J., Roemer, M. J. and Hess, A. J. (2002), "Health management system design:  
622 Development, simulation and cost/benefit optimization", *Aerospace Conference Proceedings, 2002.*  
623 *IEEE*, Vol. 6, pp. 6-3065.
- 624 [22] Rudov-Clark, S., Stecki, J. and Stecki, C. (2011), "Application of advanced failure analysis results for  
625 reliability and availability estimations", *Aerospace Conference, 2011 IEEE*, pp. 1.
- 626 [23] Elasha, F., Mba, D. and Teixeira, J. A. (2014), "Condition Monitoring Philosophy for Tidal Turbines",  
627 *International Journal of Performability Engineering*, vol. 10, no. 5, pp. 521.
- 628 [24] Paul, D. (2012), *Why gearboxes fail and solution to lower derive train cost*, available at:  
629 [http://www.windpowerengineering.com/maintenance/why-gearboxes-fail-and-a-solution-to-](http://www.windpowerengineering.com/maintenance/why-gearboxes-fail-and-a-solution-to-lower-drivetrain-costs/)  
630 [lower-drivetrain-costs/](http://www.windpowerengineering.com/maintenance/why-gearboxes-fail-and-a-solution-to-lower-drivetrain-costs/) (accessed October/14).
- 631 [25] Tidal Energy Ltd. (Tidal Energy Ltd, Cardiff, UK), (2009), *Ramsay Sound Current data UK*.

- 632 [26] Mba, D. (2005), "Prognostic opportunities offered by acoustic emission for monitoring bearings and  
633 gearboxes", *Twelfth international congress on sound and vibration*, .
- 634 [27] Reuben, L. C. K. and Mba, D. (2014), "Diagnostics and prognostics using switching Kalman filters",  
635 *Structural Health Monitoring*, vol. 13, no. 3, pp. 296-306.
- 636 [28] Aslantaş, K. and Taşgetiren, S. (2004), "A study of spur gear pitting formation and life prediction",  
637 *Wear*, vol. 257, no. 11, pp. 1167-1175.
- 638 [29] Pecht, M. and Jaai, R. (2010), "A prognostics and health management roadmap for information and  
639 electronics-rich systems", *Microelectronics Reliability*, vol. 50, no. 3, pp. 317-323.
- 640 [30] British Standards, ( 2006), *Calculation of load capacity of spur and helical gears - Part 1: Basic  
641 principle, introduction and general influence factors BS ISO 6336-1*, BSI, UK.
- 642 [31] British Standards, ( 2006), *Calculation of load capacity of spur and helical gears - Part 6: Calculation  
643 of service life under variable load BS ISO 6336-6*, BSI, UK.
- 644 [32] British Standards, ( 2006), *Calculation of load capacity of spur and helical gears - Part 2: Calculation  
645 of tooth contact strength (BS ISO 6336-2)*, BSI, UK.
- 646 [33] British Standards, ( 2006), *Calculation of load capacity of spur and helical gears - Part 3: Calculation  
647 of tooth bending strength (BS ISO 6336-3)*, UK.
- 648 [34] P., R. (2012), *Dudley's Handbook of Practical Gear Design and Manufacture*, second ed, CRC press,  
649 USA, ISBN 9781439866016.
- 650 [35] Cotrell, J. R. (2002), "A preliminary evaluation of a multiple-generator drivetrain configuration for  
651 wind turbines", *ASME 2002 Wind Energy Symposium*, American Society of Mechanical Engineers, pp.  
652 345.
- 653 [36] Smolders, K., Long, L., Feng, Y. and Tavner, P. J. (2010), "Reliability Analysis and Prediction of Wind  
654 Turbine Gearboxes", *European Wind Energy Conference*, 20-23 April 2010, Warsaw, Poland, UK, .
- 655 [37] Christopher, A. W. (2006), *Wind Turbine Reliability: Understanding and Minimizing Wind Turbine  
656 Operation and Maintenance Costs*, SAND2006-1100, Sandia National Laboratories, New Mexico ,  
657 California.
- 658 [38] Ragheb, A. and Ragheb, M. (2010), "Wind turbine gearbox technologies", *1st International Nuclear  
659 & Renewable Energy Conference (INREC)*, 21-24 March, Amman, IEEE, pp. 1.
- 660 [39] Sheng, S. and Veers, P. S. (2011), "Wind turbine drivetrain condition monitoring-an overview",  
661 *Mechanical Failures Prevention Group: Applied Systems Health Management Conference*, 10-12 May,  
662 National Renewable Energy Laboratory, Virginia, USA, pp. 2.

- 663 [40] Culley, D. M., Funke, S. W., Kramer, S. C. and Piggott, M. D. (2016), "Integration of cost modelling  
664 within the micro-siting design optimisation of tidal turbine arrays", *Renewable Energy*, vol. 85, pp.  
665 215-227.
- 666 [41] Batten, W., Bahaj, A., Molland, A. and Chaplin, J. (2007), "Experimentally validated numerical  
667 method for the hydrodynamic design of horizontal axis tidal turbines", *Ocean Engineering*, vol. 34,  
668 no. 7, pp. 1013-1020.
- 669 [42] Shen, W. Z., Mikkelsen, R., Sørensen, J. N. and Bak, C. (2005), "Tip loss corrections for wind turbine  
670 computations", *Wind Energy*, vol. 8, no. 4, pp. 457-475.
- 671 [43] Masters, I., Chapman, J., Orme, J. and Willis, M. (2011), "A robust blade element momentum theory  
672 model for tidal stream turbines including tip and hub loss corrections", *Proceedings of IMarEST-Part  
673 A-Journal of Marine Engineering and Technology*, vol. 10, no. 1, pp. 25-35.
- 674 [44] Burton, T., Jenkins, N., Sharpe, D. and Bossanyi, E. (2011), *Wind energy handbook*, Second ed, John  
675 Wiley & Sons, UK, ISBN 978-0-470-69975-1.
- 676 [45] Jarrin, N., Benhamadouche, S., Laurence, D. and Prosser, R. (2006), "A synthetic-eddy-method for  
677 generating inflow conditions for large-eddy simulations", *International Journal of Heat and Fluid  
678 Flow*, vol. 27, no. 4, pp. 585-593.
- 679 [46] Simpson, J. H., Fisher, N. R. and Wiles, P. (2004), "Reynolds stress and TKE production in an estuary  
680 with a tidal bore", *Estuarine, Coastal and Shelf Science*, vol. 60, no. 4, pp. 619-627.
- 681 [47] Lu, Y. and Lueck, R. G. (1999), "Using a broadband ADCP in a tidal channel. Part II: Turbulence",  
682 *Journal of Atmospheric and Oceanic Technology*, vol. 16, no. 11, pp. 1568-1579.
- 683 [48] Thomson, J., Polagye, B., Durgesh, V. and Richmond, M. C. (2012), "Measurements of turbulence  
684 at two tidal energy sites in Puget Sound, WA", *Oceanic Engineering, IEEE Journal of*, vol. 37, no. 3,  
685 pp. 363-374.
- 686 [49] Tedds, S., Owen, I. and Poole, R. (2014), "Near-wake characteristics of a model horizontal axis tidal  
687 stream turbine", *Renewable Energy*, vol. 63, pp. 222-235.
- 688 [50] Khan, M. A., Cooper, D. and Starr, A. (2009), "BS-ISO Helical Gear Fatigue Life Estimation and Wear  
689 Quantitative Feature Analysis", *Strain*, vol. 45, no. 4, pp. 358-363.
- 690 [51] Milne, I. A., Sharma, R. N., Flay, R. G. and Bickerton, S. (2013), "Characteristics of the turbulence in  
691 the flow at a tidal stream power site", *Philosophical transactions. Series A, Mathematical, physical,  
692 and engineering sciences*, vol. 371, no. 1985, pp. 20120196.
- 693 [52] ISO standard, ( 2013), *ISO 12110-2:2013 Metallic materials -- Fatigue testing -- Variable amplitude  
694 fatigue testing -- Part 2: Cycle counting and related data reduction methods*, the International  
695 Organization for Standardization.

696 [53] Link, H., Lacava, W., Van Dam, J., McNiff, B., Sheng, S., Wallen, R., MCdade, M., Lambert, S.,  
697 Butterfield, S. and Oyague, F. (2011), *Gearbox Reliability Collaborative Project Report: findig from*  
698 *phase 1 and phase 2 testing*, NREL/TP-5000-51885, National Renewable Energy Laboratory, USA.

699

700

701

702

ACCEPTED MANUSCRIPT

## Highlights

- Failures in gearboxes are essentially related to the uncertainty associated with loading condition during the design phase.
- A prognostic model based on the loading condition has been developed to predict the residual life of a gearbox during turbine operation.
- The model employed synthetic turbulence data generated for The Ramsey Sound region
- The result shows life variations between the gears.
- The model was validated using pitting test data and an accurate prediction of life was proved